

THE ROLE OF MAJOR GAS-RICH MERGERS ON THE EVOLUTION OF GALAXIES FROM THE BLUE CLOUD TO THE RED SEQUENCE

Rui Guo^{1,2,3}, Cai-Na Hao³, X. Y. Xia³, Shude Mao^{4,2,5}, Yong Shi^{6,7}

ABSTRACT

With the aim of exploring the fast evolutionary path from the blue cloud of star-forming galaxies to the red sequence of quiescent galaxies in the local universe, we select a local advanced merging infrared luminous and ultraluminous galaxy (adv-merger (U)LIRGs) sample and perform careful dust extinction corrections to investigate their positions in the SFR- M_* , $u-r$ and $NUV-r$ color-mass diagrams. The sample consists of 89 (U)LIRGs at the late merger stage, obtained from cross-correlating the *IRAS* Point Source Catalog Redshift Survey and 1 Jy ULIRGs samples with the Sloan Digital Sky Survey DR7 database. Our results show that $74\% \pm 5\%$ of adv-merger (U)LIRGs are localized above the 1σ line of the local star-forming galaxy main sequence. We also find that all adv-merger (U)LIRGs are more massive than and as blue as the blue cloud galaxies after corrections of Galactic and internal dust extinctions, with $95\% \pm 2\%$ and $81\% \pm 4\%$ of them outside the blue cloud on the $u-r$ and $NUV-r$ color-mass diagrams, respectively. These results, combined with the short timescale for exhausting the molecular gas reservoir in adv-merger (U)LIRGs (3×10^7 to 3×10^8 years), imply that the adv-merger (U)LIRGs are likely at the starting point of the fast evolutionary track previously proposed by several groups. While the number density

¹National Astronomical Observatories, Chinese Academy of Sciences, 20A Datun Road, Chaoyang District, Beijing 100012, China

²University of Chinese Academy of Sciences, Beijing 100049, China

³Tianjin Astrophysics Center, Tianjin Normal University, Tianjin 300387, China; E-mail: cainahao@gmail.com

⁴Physics Department and Tsinghua Center for Astrophysics, Tsinghua University, Beijing, 100084, China

⁵Jodrell Bank Centre for Astrophysics, University of Manchester, Alan Turing Building, Manchester M13 9PL, UK

⁶School of Astronomy and Space Science, Nanjing University, Nanjing 210093, China

⁷Key Laboratory of Modern Astronomy and Astrophysics, Nanjing University, Ministry of Education, Nanjing 210093, China

of adv-merger (U)LIRGs is only $\sim 0.1\%$ of the blue cloud star-forming galaxies in the local universe, this evolutionary track may play a more important role at high redshift.

Subject headings: galaxies: evolution - galaxies: formation - galaxies: interactions
- galaxies: starburst - infrared: galaxies

1. INTRODUCTION

Galaxies show a striking color bimodality in the color-magnitude and the color-stellar mass (color-mass, hereafter) diagrams, both locally, based on the Sloan Digital Sky Survey (SDSS) (Kauffmann et al. 2003b; Baldry et al. 2004, 2006), and at high redshift (Bell et al. 2004; Faber et al. 2007; Ilbert et al. 2010). Since the discovery of the bimodality, several evolutionary pathways have been proposed for how the blue cloud of star-forming galaxies evolves to the red sequence of quiescent galaxies through the transition phase of the so-called green valley (e.g. Bell et al. 2004; Faber et al. 2007; Marchesini et al. 2014; Schawinski et al. 2014).

There is also a tight correlation between the star formation rate (SFR) and the stellar mass for normal star-forming galaxies, which is referred to as the “main sequence” (MS) and changes with redshift in its normalization out to redshift 6 (e.g. Brinchmann et al. 2004; Elbaz et al. 2007; Noeske et al. 2007; Leitner 2012; Magdis et al. 2010; Bouwens et al. 2012; Salmon et al. 2015). Meanwhile, starburst galaxies are located above the MS and are likely driven by gas-rich major mergers (Rodighiero et al. 2011; Hung et al. 2013).

Furthermore, based on CO observations for galaxies at both low and high redshifts, Daddi et al. (2010) and Genzel et al. (2010) presented evidence for the bimodal behavior of star formation processes. Disk galaxies and starburst galaxies, triggered by gas-rich major mergers, occupy distinct regions in the SFR and gas mass diagrams. They suggested two star formation modes: a long-lasting star formation mode where the gas reservoir is consumed slowly for disk galaxies, and a rapid star formation mode for starburst galaxies which have high star formation efficiencies (~ 10 times higher than those of disk galaxies) due to their much higher dense gas fractions (Gao & Solomon 2004). It is likely that there exists a close link between the two star formation modes and the different evolutionary pathways.

In recent years, there are many works investigating the bimodality of galaxies in the color-magnitude diagram, particularly on how the blue cloud star-forming galaxies are quenched and evolve to the red sequence (quiescent) galaxies with a broad stellar mass distribution. This is especially the case for the formation of massive quiescent galaxies. From the results

of DEEP2 and COMBO-17 surveys on the luminosity functions of blue and red galaxies to redshift 1, Faber et al. (2007) first proposed a mixed scenario for the formation of massive red quiescent galaxies. They suggested that after star formation in the blue cloud galaxies is quenched, these galaxies leave the blue cloud and migrate to the red sequence, then they evolve slowly along the red sequence through a series of dry mergers to form local massive red sequence galaxies. On the other hand, observations of high-redshift galaxies (van Dokkum et al. 2008; Kriek et al. 2009) found that massive quiescent galaxies are substantially more compact than local galaxies with similar stellar masses. Galaxies with intense and concentrated starbursts, triggered by gas-rich major mergers, are possible progenitors of massive compact quiescent galaxies (Wellons et al. 2015). Actually, Barro et al. (2013) detected compact star-forming galaxies (cSFGs) at redshift 1.4-3 by combining high resolution HST/WFC3 images and multi-wavelength photometry of massive galaxies ($M_* \geq 10^{10} M_\odot$) in GOODS-S and UDS fields of the Cosmic Assembly Near-infrared Deep Extragalactic Legacy Survey (CANDELS; Grogin et al. 2011; Koekemoer et al. 2011). From the number densities, sizes, SFRs and dynamical properties of cSFGs, they are likely the progenitors of high-redshift compact quiescent massive galaxies (cQGs, see also Barro et al. 2014a, 2014b). Then, Barro et al. (2013) proposed two evolutionary tracks to form quiescent galaxies: the cSFGs formed by gas-rich processes are quenched rapidly and fade to compact massive early-type galaxies, subsequent minor dry mergers can puff up quiescent early-type galaxies over time and grow in the quiescent phase; on the other hand, larger SFGs evolve slowly and become extended early-type galaxies directly.

More and more pieces of evidence support this two evolutionary pathway scenario, especially the fast track for the formation of massive quiescent galaxies. Marchesini et al. (2014) searched for the progenitors of local ultra-massive galaxies with $M_* > 6 \times 10^{11} M_\odot$ based on Ultra VISTA catalogs (Muzzin et al. 2013b) and concluded that the progenitors of red sequence massive galaxies are red, massive and heavily dust-extincted starburst galaxies and have never been on the blue cloud since redshift 3. It implies that the most massive galaxies formed early and quickly, which has been confirmed by Mancini et al. (2015) based on detailed investigation for 56 massive galaxies on an object-to-object basis in the GOODS-South field at $1.4 < z < 2$. Combining the SDSS Data Release 7 (DR7; York et al. 2000; Abazajian et al. 2009) and the *Galaxy Evolution Explorer (GALEX)* databases (Martin et al. 2005), and using the morphology of galaxies from the Galaxy Zoo project (Lintott et al. 2008; Lintott et al. 2011), Schawinski et al. (2014) found that the bimodality of galaxies in the color-mass diagram changes dramatically, i.e., there is not a clear green valley dip for both late-type and early-type galaxies. A further analysis for the green valley galaxies based on the UV-optical colors shows that for the majority of late-type galaxies, their star formation rates decline secularly over several Gyr. In contrast, only a small fraction of blue galaxies

evolve rapidly to the red sequence by gas-rich mergers and transform from disk galaxies to spheroids that should be the recently quenched massive blue galaxies found by McIntosh et al. (2014) based also on SDSS database. Most recently, Belli et al. (2015) investigated 62 massive galaxies at the redshift range $1 < z < 1.6$ based on Keck LRIS spectra and confirmed the fast quenching mode that is through post-starburst phase. Actually, Yesuf et al. (2014) analyzed a sample of post-starburst galaxies and concluded that the quenching mechanisms could be broadly classified as fast and slow tracks. The rapid quenching (the fast track) in the local universe is triggered by merger-induced starbursts. Therefore, it is worth studying the fast quenching process in detail from a local gas-rich major merging galaxy sample.

In fact, such a sample is already known: almost all local ultraluminous infrared galaxies (ULIRGs; $L_{\text{IR}}^1 > 10^{12} L_{\odot}$) and a large fraction of luminous infrared galaxies (LIRGs; $10^{11} L_{\odot} < L_{\text{IR}} < 10^{12} L_{\odot}$) are gas-rich interacting/merging galaxies (e.g. Sanders & Mirabel 1996; Wang et al. 2006; Kaviraj 2009). Such gas-rich major mergers funnel cold molecular gas reservoirs into the centers, leading to massive starbursts (Downes & Solomon 1998). Their stellar masses are moderate (Dasyra et al. 2006a, 2006b; da Cunha et al. 2010; also see Section 4.2), but are higher than those of blue cloud galaxies ($M_{*} < 3 \times 10^{10} M_{\odot}$) (Kauffmann et al. 2004). Similarly, a large fraction of high-redshift ULIRGs are interacting/merging and starburst galaxies (Kartaltepe et al. 2010, 2012; Zamojski et al. 2011; Soto & Martin 2012; Hung et al. 2014; Yan et al. 2014). Furthermore, Casey et al. (2014) found that the dusty star-forming galaxies with SFRs above $50 M_{\odot} \text{ yr}^{-1}$ (LIRGs and ULIRGs) are blue at both low and high redshifts and become bluer as their infrared luminosity increases. Since LIRGs and ULIRGs are blue and have higher stellar masses than the blue cloud disk galaxies, these galaxies should occupy the bottom right corner of the color-mass diagram and may be the progenitors of massive red sequence galaxies. In fact, Chen et al. (2010) have investigated the positions of 52 local ULIRGs in the $g-r$ color-magnitude diagram without applying internal extinction corrections, and found that $\sim 46\%$ ULIRGs lie outside the 90% level number density contour, with a few in the green valley or even on the red sequence. Kilerci Eser et al. (2014) obtained similar results with a larger sample of 82 local ULIRGs. If the galaxy internal extinction is corrected, these local ULIRGs would appear even bluer and brighter, possibly occupying different locations in the color-magnitude and color-mass diagrams. For this purpose, we select a local (U)LIRG sample and focus on those with advanced merging (adv-merger, hereafter) morphologies, which are galaxies at the late gas-rich major merger stage with a single nucleus. Furthermore, we perform the galaxy internal extinction correction carefully and investigate how their locations change in the SFR-mass and color-mass diagrams.

¹ L_{IR} is the integrated infrared luminosity between 8-1000 μm .

The structure of this paper is as follows. In Sections 2 and 3 we describe the sample selection and parameters estimation for our sample adv-mergers and control samples. In Section 4, we present our main results. We discuss and summarize in Sections 5 and 6 respectively. Throughout this paper we adopt the Kroupa (2001) initial mass function and a cosmological model of $H_0 = 70 \text{ km s}^{-1} \text{ Mpc}^{-1}$, $\Omega_m = 0.3$ and $\Omega_\Lambda = 0.7$.

2. SAMPLE SELECTION

2.1. Advanced Mergers

We morphologically select advanced mergers from a SDSS r -band limited sample of LIRGs and ULIRGs, most of which are in the redshift range of $z < 0.1$ and $0.1 < z < 0.25$, respectively. Specifically, our dusty adv-merger sample is mainly drawn from the cross-correlation between the spectroscopic catalog of SDSS DR7 (York et al. 2000; Abazajian et al. 2009) and the *Infrared Astronomical Satellite (IRAS)* Point Source Catalog Redshift Survey (PSCz, Saunders et al. 2000), during which we used a $5''$ searching radius. Given that ULIRGs are very rare in the local universe ($z < 0.3$)² but most of them are in the late merging stage (e.g. Sanders & Mirabel, 1996; Veilleux et al. 2002), the ULIRGs in our sample are mainly collected by searching for counterparts of the *IRAS* 1 Jy ULIRGs sample (Kim & Sanders 1998) in the SDSS DR7 photometric catalog. We describe the sample selection procedures in more detail below.

Since reliable morphological classifications can only be achieved for SDSS galaxies brighter than 15.9 mag in the r -band (Fukugita et al. 2004) and the spectroscopic observations are incomplete for SDSS galaxies with r -band magnitude brighter than 14.5 mag (Kauffmann et al. 2003b), we restricted our infrared luminous and ultraluminous galaxy sample to a magnitude range of $14.5 < r < 15.9$ after corrections for foreground Galactic extinction (Schlegel et al. 1998). Within this magnitude range, 259 LIRGs and ULIRGs were obtained by the cross-correlation between the SDSS DR7 and PSCz. We will discuss possible selection effects caused by this magnitude cut in Section 4.2.1. Furthermore, we examined the positions of SDSS fibers on the images for these galaxies, and found that for 6 galaxies the fiber spectra were obtained for off-center regions. Considering that the SFR might be under-estimated by the $\text{H}\alpha$ emission line for these galaxies, we removed them from our sample. This step reduced the number of galaxies to 253, out of which there are only 3 ULIRGs. Therefore, we perform further cross-correlation between the photometric catalog

²There is only one ULIRGs within redshift 0.03 (Sanders & Mirabel, 1996).

of SDSS DR7 and the *IRAS* 1 Jy ULIRGs sample, yielding 63 ULIRGs, among which there are 39 objects with SDSS spectra. As the morphologies of these ULIRGs have been well studied in the literature, we did not put constraints on their *r*-band magnitudes. In total, the sample consists of 314 LIRGs and ULIRGs after excluding 2 overlapping objects in the above two cross-correlation procedures.

Considering that we are only concerned with the adv-mergers in this work, we further performed morphological classifications for the above 314 galaxies visually. The classification scheme is similar to that of Wang et al. (2006). The visual classifications are primarily based on their *r*-band images from SDSS DR7 or *K*-band images from the 2.2 m telescope of University of Hawaii (Kim et al. 2002). Then we used SDSS composite true color images by combining *g*, *r*, *i* filter data as cross-check (Lupton et al. 2004). The sample galaxies are classified into five classes: early-type like galaxies with relaxed morphologies (12), spiral galaxies with bars or without bars (118), interacting galaxies with disturbed morphologies (55), pre-merging galaxies with two or more nuclei (27) and advanced merging galaxies (adv-merger) with a single nucleus but some merger signs (100). Furthermore, we compared our morphological classification results with the Galaxy Zoo 1³ (Lintott et al. 2008; Lintott et al. 2011). There are just a few different classifications ($\sim 10\%$), in which some interacting or merging galaxies in our classifications were classified as spirals or ellipticals in the Galaxy Zoo, but their images do show disturbed features. Our classifications for early-type and spiral galaxies are almost the same as those of Galaxy Zoo. We only select the 100 adv-merging galaxies as our working sample. Figure 1 shows the true color images of 8 example adv-mergers.

Since spectral information is needed in our subsequent analysis, one ULIRG without such information was excluded. In addition, we removed 10 objects with Seyfert 1 spectra from our sample, as the estimations for their extinctions, stellar masses and star formation rates are unreliable. Thus our final adv-merger sample consists of 89 galaxies (60 LIRGs and 29 ULIRGs). According to the commonly used spectral classification BPT diagram proposed by Baldwin et al. (1981) and developed by Kauffmann et al. (2003a) and Kewley et al. (2001) based on $[\text{N II}] \lambda 6584/\text{H}\alpha$ versus $[\text{O III}] \lambda 5007/\text{H}\beta$, we classified our sample galaxies into 25 star-forming galaxies, 42 composite galaxies and 20 narrow-line AGNs (including Seyfert 2 and low-ionization narrow emission-line region galaxies). For the remaining two galaxies, the line fluxes have signal-to-noise ratios too low ($\text{S/N} < 5$) to be classified reliably. The black line and gray shaded histograms in Figure 2 represent the redshift (left panel) and infrared luminosity (right panel) distributions for the 314 (U)LIRGs before morphological

³ <http://data.galaxyzoo.org/>

classification and the 89 sample adv-merger (U)LIRGs, respectively. In the left panel of Figure 2, we also overplot the redshift distributions of LIRGs (blue line) and ULIRGs (red line) separately. It can be seen that the lower redshift region ($z < 0.1$) is dominated by LIRGs and the higher redshift region ($0.1 < z < 0.25$) is occupied by ULIRGs.

2.2. Control Samples

For consistent estimates of physical parameters between our working sample and the comparison samples, we do not use published relations in the literature. Instead, we constructed the control samples by ourselves. The control sample used to investigate the SFR- M_* relation for star-forming galaxies has been extracted from the SDSS DR7 and satisfies $0.005 < z < 0.2$ and $14.5 < r < 17.77$. The star-forming galaxies were selected according to the BPT diagram given by Kauffmann et al. (2003a). The sample selection procedure is similar to that of Brinchmann et al. (2004). This leaves us with 152137 galaxies. For the color-mass relation, the control sample was retrieved from the Oh-Sarzi-Schawinski-Yi (OSSY) catalog (Oh et al. 2011)⁴, which is a spectroscopically selected galaxy sample from the SDSS DR7 with redshifts $z < 0.2$. It provides internal extinction information ($E(B-V)$) from stellar continuum fits (EBV_STAR). For comparison with Schawinski et al. (2014) in the color-mass relation studies, we further restricted the redshift of the comparison sample to $0.02 < z < 0.05$ and luminosity $M_{z,\text{Petro}} < -19.5$ mag to obtain an approximately mass-limited sample as described in Schawinski et al. (2014). The final control sample consists of 53604 galaxies.

3. PARAMETER ESTIMATIONS

In this paper, we mainly investigate the positions of adv-merger (U)LIRGs in the SFR-stellar mass and the color-stellar mass diagrams. Hence we need to carefully estimate the star formation rates, dust extinction corrected $u-r$, $NUV-r$ colors, as well as stellar masses for our sample adv-mergers and the control sample galaxies.

The optical photometric data are all from SDSS DR7, while the near ultraviolet (NUV) magnitudes are from the *GALEX* satellite (Martin et al. 2005). There are 79 sample adv-mergers and $\sim 87\%$ control sample galaxies with NUV photometric data available from the *GALEX*. We first performed k -corrections to the optical and NUV magnitudes, followed

⁴ <http://gem.yonsei.ac.kr/~ksoh/wordpress>

by the Galactic extinction and internal extinction corrections. The k -corrections to the optical and NUV magnitudes were performed using the New York University Value-Added Galaxy Catalog (NYU-VAGC; Blanton & Roweis 2007) and by the IDL routine `calc_kcor.pro`⁵ (Chilingarian et al. 2010; Chilingarian & Zolotukhin 2012), respectively. The foreground Galactic extinctions were corrected using dust maps from Schlegel et al. (1998). For the galaxies with SDSS spectroscopic information, the EBV_STAR values from the OSSY catalog (Oh et al. 2011) have been directly used to correct for the internal dust extinctions. However, for 10 ULIRGs not in the SDSS spectroscopic catalog and thus not in the OSSY catalog, we had to perform internal extinction corrections ourselves, which is described as follows. First, we calculated the color excess in the gas (EBV_GAS) for the ULIRGs in the SDSS spectroscopic survey using Balmer decrements $H\alpha/H\beta$, assuming the case B recombination value of intrinsic $H\alpha/H\beta$ as 2.86 and 3.1 for star-forming galaxies and AGNs, respectively (Osterbrock & Ferland 2006). Second, we obtained the relation between EBV_STAR and EBV_GAS for these galaxies: $EBV_STAR = -0.03 + 0.61EBV_GAS$. Finally, we retrieved the Balmer decrements for those ULIRGs without SDSS spectra from literature (Veilleux et al. 1999; Darling et al. 2006) to calculate EBV_GAS and derived their EBV_STAR using the EBV_STAR and EBV_GAS relation fitted above. At the last step, the dust extinction corrected $u-r$ colors and NUV magnitudes for all sample galaxies were obtained using the Calzetti et al. (2000) extinction law and Cardelli et al. (1989) law, respectively, following Schawinski et al. (2014). For our adv-merger sample, the median internal extinction is 0.89 mag for the $u-r$ color.

The stellar masses for most sample adv-mergers and all the control sample galaxies were retrieved from the Max Planck Institute for Astrophysics-Johns Hopkins University (MPA/JHU⁶) stellar mass catalog (Kauffmann et al. 2003b), which were estimated using the SDSS five broad-band photometry. Briefly, a median likelihood estimate of the stellar mass was derived by comparing the five broad-band photometry with the synthetic photometry of a large library of model star formation histories using the Bayesian methodology. This library of model star formation histories includes bursting and continuous star formation histories and covers a wide range in metallicity. In other words, this method has already taken proper star formation histories into account during the modeling. So for both galaxies with bursting star formation histories and those with continuous star formation histories, the stellar mass estimates should not suffer from systematical impact from improper assumptions of their star formation histories. For galaxies not included in the MPA/JHU stellar mass catalog, 10 out of 89 sample galaxies, we calculated the stellar masses following Bell et al.

⁵<http://kcor.sai.msu.ru/>

⁶<http://www.mpa-garching.mpg.de/SDSS>

(2003), utilizing the equation

$$\log(M_*/M_\odot) = -0.4(M_{r,AB} - 4.67) + [a_r + b_r(g - r)_{AB} - 0.15], \quad (1)$$

where M_*/M_\odot is the stellar mass in solar units, $M_{r,AB}$ is the r -band absolute magnitude in the AB magnitude system and $(g - r)_{AB}$ is the color in the rest-frame. The coefficients a_r and b_r are taken as -0.306 and 1.097 , respectively, and the term -0.15 is adopted for the Kroupa initial mass function (see Bell et al. 2003). To check the consistency between these two methods, we computed the stellar masses for the galaxies included in the MPA/JHU stellar mass catalog using Equation (1). The median difference of the two approaches is 0.03 dex. Therefore, the equation of Bell et al. (2003) can be used statistically to measure the stellar masses for galaxies not in the MPA/JHU catalog. Even though, we still use stellar masses taken from MPA/JHU for most sample galaxies in this work, because for our dusty starburst galaxies the stellar mass based on five broad-band photometry and using the way described above should be more reliable for individual galaxy than that using only two band photometry by Bell et al. (2003).

Given that all our sample adv-mergers are infrared luminous and selected from the *IRAS* database, the star formation rate can be derived from their total infrared luminosity, following Kennicutt (1998, K98 hereafter)

$$\text{SFR(IR)}(M_\odot \text{ yr}^{-1}) = 4.5 \times 10^{-44} L_{\text{IR}}(\text{ergs s}^{-1}). \quad (2)$$

On the other hand, we can also calculate the star formation rate for star-forming and composite adv-mergers and 152137 star-forming control sample galaxies using their $\text{H}\alpha$ luminosities retrieved from the MPA/JHU catalog following K98

$$\text{SFR(H}\alpha\text{)}(M_\odot \text{ yr}^{-1}) = 7.9 \times 10^{-42} L(\text{H}\alpha)(\text{ergs s}^{-1}). \quad (3)$$

The $\text{H}\alpha$ luminosities are aperture-corrected using the difference of the r -band Petrosian magnitude to the fiber magnitude (Hopkins et al. 2003) as well as dereddened assuming the case B recombination value of intrinsic $\text{H}\alpha/\text{H}\beta$ as 2.86. Note that in the above formulae, the Salpeter (1955) initial mass function has been used and we converted them to the Kroupa one by dividing a factor 1.5.

4. RESULTS

4.1. The SFR-Stellar Mass Relation

It is generally accepted that star-forming galaxies lie on the MS of the SFR- M_* relation while starburst galaxies are located above the MS (Rodighiero et al. 2011; Hung et al.

2013). Below we investigate where our sample adv-mergers are located in the same diagram to obtain clues on their evolution.

Figure 3 shows the $\text{SFR}(\text{IR})-M_*$ relation for 89 sample adv-mergers. The ULIRGs and LIRGs are shown as red and blue filled circles, respectively. The black solid and dashed lines in Figure 3 represents the best fit MS relation and 1σ scatter after 3σ clipping of outliers, respectively, based on 152137 star-forming galaxies selected from SDSS DR7 (see Section 2.2) as

$$\log \text{SFR}(\text{H}\alpha) = (1.02 \pm 0.001) \log(M_*/M_\odot) - (10.01 \pm 0.014). \quad (4)$$

The 1σ dispersion of our fitting MS relation is 0.3 dex after the typical SFR estimation scatter ~ 0.2 dex is removed, which is consistent with the scatters derived in the literature (e.g. Noeske et al. 2007; Rodighiero et al. 2011; Whitaker et al. 2012; Sargent et al. 2012). Note that for the normal star-forming galaxies used to fit the MS relation, their SFRs are calculated with their $\text{H}\alpha$ luminosities, which are consistent with those estimated from their infrared luminosities (Kennicutt et al. 2009; Lee et al. 2013).

It is clear from Figure 3 that almost all adv-merger (U)LIRGs are above MS line and a large fraction ($74\% \pm 5\%$) of them are localized above the 1σ line of MS relation. In particular, the ULIRGs are far above the MS line as outliers, consistent with previous findings (e.g. Elbaz et al. 2007; da Cunha et al. 2010). The fraction of LIRGs above MS relation is also high ($62\% \pm 6\%$). Given that the definition of starburst galaxies based on deviations from the MS relation varies in the literature (Rodighiero et al. 2011; Hung et al. 2013), in this work we define starburst galaxies as those above the 1σ line of MS relation. Then more than two-thirds (74%) of our sample adv-merger (U)LIRGs are in the starburst phase. In practice, this definition of starburst is also consistent with starburst definitions based on other starburst indicators, such as high star formation rates and short molecular gas exhausting timescales (Knapen & James 2009; see Section 5.3).

4.2. The Color-Stellar Mass Relation

4.2.1. The $u-r$ Color-Mass Relation

Since our goal is to investigate the role of gas-rich major mergers on galaxy evolution from the blue cloud to the red sequence of quiescent galaxies in the color-mass diagram, accurate dust extinction correction is very important. Schawinski et al. (2014) found that the galaxies in the blue cloud are bluer in the dust extinction corrected color-mass diagram compared with the uncorrected one, leading to a more prominent blue cloud and red sequence. For our adv-merger (U)LIRGs sample, dust extinction is even more serious: the median

internal extinction is 0.89 mag on the $u-r$ color as derived in Section 3. Therefore, we performed both foreground Galactic and galaxy internal extinction corrections carefully.

Figure 4 illustrates the foreground Galactic and internal dust extinction corrected $u-r$ color-mass diagram. In the left panel of Figure 4, the gray dots represent 53604 comparison sample galaxies (see Section 2.2), and the overlaid contours show the galaxy number densities for these galaxies. The lowest density contour represents the 90% number density. The control sample galaxies show an obvious bimodal distribution as the blue cloud and the red sequence. The area in between is the green valley. The two black lines in Figure 4 denote its boundaries, which are similar to the definition of Schawinski et al. (2014)

$$u - r = -0.24 + 0.25 \log(M_*/M_\odot), \quad (5)$$

$$u - r = -0.75 + 0.25 \log(M_*/M_\odot). \quad (6)$$

Note that the black lines shown in Figure 4 are 0.07 mag bluer than the above definition to account for the Galactic extinction corrections we performed. The median Galactic extinction for the comparison sample is ~ 0.07 mag. Since the boundary definition of the green valley is somewhat arbitrary, the adjustment we took is more suitable for the galaxy distribution in the color-mass diagram shown in Figure 4 than those given by Equations (5) and (6).

The red and blue filled circles in the left panel of Figure 4 represent adv-merger ULIRGs and LIRGs, respectively. It is clear from the left panel of Figure 4 that almost all our sample galaxies are indeed localized to the right of blue cloud galaxies in the color-mass diagram and $95\% \pm 2\%$ sample galaxies are outside the lowest density contour due to their larger stellar masses and bluer colors (simply refer to “at the bottom right corner of the color-mass diagram”, hereafter). Therefore, there do exist a distinct population of galaxies that belong to neither the blue cloud, red sequence, nor the green valley. Actually, Chen et al. (2010) have already reported this population in the $g-r$ color-mass diagram for 52 local galaxies selected from *IRAS* 1 Jy ULIRG sample, but only $\sim 46\%$ of their ULIRGs are located outside the 90% number density contour. From the analysis of a larger sample with 82 local ULIRGs from cross-matching the *AKARI* all-sky survey (Murakami et al. 2007) with SDSS DR10 (Ahn et al. 2014) and the Two-Degree Field Galaxy Redshift Survey (2dFGRS; Colless et al. 2001), Kilerci Eser et al. (2014) obtained similar results to that of Chen et al. (2010). We note that both studies have not applied internal dust extinction corrections, which is the main cause for the difference in the fractions of galaxies outside the 90% density contour between this work and those of Chen et al. (2010) and Kilerci Eser et al. (2014).

We also examine the L_{IR} distribution of our adv-merger (U)LIRGs in the color-mass diagram in the right panel of Figure 4 by different colors. It is clear from the right panel of

Figure 4 that the galaxies tend to be located further away from the blue cloud area as the L_{IR} increases.

Statistical studies based on large samples have not noticed this population, implying that the fraction of such galaxies is small in the local universe. It should be interesting to have a rough order-of-magnitude estimate for the fraction. To derive this fraction, we first calculated the number density of (U)LIRGs based on the analytical infrared luminosity function (LF) provided by Goto et al. (2011). The integrated number density over the luminosity range of $10^{11}L_{\odot}$ to $10^{12.5}L_{\odot}$ is $2.1 \times 10^{-5} \text{ Mpc}^{-3}$, after converting the cosmology adopted by Goto et al. (2011) to the one used in this work. We note that the infrared luminosity function constructed by Goto et al. (2011) only probes galaxies with luminosities from $10^{9.8}L_{\odot}$ to $10^{12.5}L_{\odot}$ while many blue cloud galaxies may have infrared luminosities fainter than $10^{9.8}L_{\odot}$. So an integrated number density over this infrared luminosity range would under-estimate the total number density of blue cloud galaxies. To remedy this, we resort to an optical luminosity function to estimate the number density of blue cloud galaxies: we used the r -band luminosity function for late-type galaxies by Nakamura et al. (2003) since blue cloud galaxies are mostly late-type (Schawinski et al. 2014). The total number density in the luminosity range of $-23.3 < M_r < -18.8$, which brackets the blue cloud galaxies, is $8.2 \times 10^{-3} \text{ Mpc}^{-3}$. Consequently, the fraction of (U)LIRGs to late-type galaxies is about 0.26%. Note that although ULIRGs are almost exclusively interacting or merging systems, about half of the LIRGs are spirals (Wang et al. 2006). Therefore the real fraction of infrared luminous adv-mergers should be smaller by a factor of a few, i.e., less than 0.1%. Considering that late-type galaxies may include galaxies not in the blue cloud, this fraction may be higher than 0.1%. But it will not change in the order-of-magnitude. Such a tiny fraction suggests that blue, massive dusty galaxies at the bottom right corner of the color-mass diagram are very rare in the local universe.

Considering that we have put a constraint on the magnitude range of $14.5 < r < 15.9$ when we selected our (U)LIRGs sample by cross-correlation analysis, we should examine possible selection effects by such a magnitude cut. Figure 5 shows the comparison of $u-r$ color distributions for 259 (U)LIRGs within the magnitude range of $14.5 < r < 15.9$ (solid line) and 636 (U)LIRGs with $r > 14.5$ (dashed line). The black vertical dot-dashed line denotes the $u-r$ color for the lower boundary of the green valley at the median stellar mass of our sample galaxies. We can see from Figure 5 that almost all (U)LIRGs are blue, and the galaxies in magnitude ranges of $14.5 < r < 15.9$ and those with $r > 14.5$ cover similar ranges in $u-r$ colors, indicating that the constraint on magnitude range of $14.5 < r < 15.9$ does not preferentially select blue galaxies. In addition, the gray shaded histogram in Figure 5 represents the $u-r$ color distribution for 89 sample (U)LIRGs, from which we can see that the adv-merger (U)LIRGs are slightly bluer than the whole (U)LIRGs sample.

4.2.2. The $NUV-r$ Color-Mass Relation

It is well known that the rest-frame optical colors are sensitive to star formation on timescales of $10^8 - 10^9$ yr (K98; Hopkins et al. 2003; Moustakas et al. 2006) while the ultraviolet emission traces the star-forming process on shorter timescales of $10^7 - 10^8$ yr, thus the $NUV-r$ color is more closely related to the current star formation process (K98). Actually, Cortese (2012) found that optically red massive spirals are on the UV-optical blue cloud and concluded that it is difficult to distinguish active star-forming galaxies from truly passive ones using optical colors alone. Figure 6 shows the dust-corrected $NUV-r$ color versus stellar mass relation for 79 sample galaxies and 46407 comparison sample galaxies. We use a similar method to that used for the $u-r$ color-mass diagram to define the boundaries of the green valley in the $NUV-r$ color-mass diagram as follows:

$$NUV - r = -0.159 + 0.492 \log(M_*/M_\odot), \quad (7)$$

$$NUV - r = -2.259 + 0.492 \log(M_*/M_\odot). \quad (8)$$

In comparison with Figure 4, the separation of the blue cloud and the red sequence is more prominent and the green valley covers a wider range in $NUV-r$, which is consistent with previous studies (Martin et al. 2007; Salim et al. 2007; Schiminovich et al. 2007; Wyder et al. 2007). Upon a closer examination of the relative positions of our sample galaxies to the blue cloud, we find a difference from those shown in Figure 4. Although most ($81\% \pm 4\%$) of our sample galaxies are still localized at the bottom right of the $NUV-r$ color-mass diagram and do not reside in the blue cloud, a few sample galaxies show up in the green valley in the $NUV-r$ color-mass diagram.

5. DISCUSSION

5.1. Stellar Mass Estimates for (U)LIRGs

The stellar mass is a fundamental quantity and is a key parameter in this work. The stellar masses of our sample galaxies are estimated via SED modeling. Due to the complex star formation histories of young stellar populations in (U)LIRGs (e.g. Rodríguez Zaurín et al. 2007, 2008), the stellar masses of (U)LIRGs estimated via SED modeling may have large uncertainties and systematic biases.

We compare the stellar masses estimated in this work with the dynamical masses of ULIRGs by Dasyra et al. (2006a, 2006b). Dasyra et al. (2006a, 2006b) provided the largest ULIRG sample (54) with dynamical mass measurements, based on high resolution, long-slit

H- and *K*- band spectroscopy. Their sample consists of 31 single nucleus and 23 double nuclei ULIRGs. We retrieve the dynamical masses from Dasyra et al. (2006a, 2006b) for 10 ULIRGs that overlap with our sample. The left panel of Figure 7 compares the stellar masses of the 10 ULIRGs measured by their SEDs with their dynamical masses derived from CO ro-vibrational line measurements. Although the sample size is small, it is obvious that the stellar masses and the dynamical masses are consistent with each other and the largest difference is only 0.3 dex. In the inset, we compare the distributions of stellar masses for our sample ULIRGs and the dynamical masses of 31 single nucleus ULIRGs retrieved from Dasyra et al. (2006b). These two distributions are quite similar with nearly identical median logarithmic values (10.86 and 10.91, respectively), and the K-S test gives a probability of 0.67, indicating that the differences between these two distributions are not statistically significant. Therefore, it appears that the stellar masses measured via SED modeling are reliable for local ULIRGs.

To extend the size of sample (U)LIRGs with dynamical masses (M_{dyn}), we also estimate the dynamical masses approximately by $M_{\text{dyn}} = 5r_{50} \sigma^2 / G$ (e.g., Bernardi et al. 2010), where the velocity dispersion (σ) and the Sérsic half-light radius r_{50} are retrieved from the MPA/JHU catalog and NYU-VAGC (Blanton et al. 2005), respectively. After excluding the objects with low signal-to-noise ratios ($S/N < 10$) and with velocity dispersions less than 70 km/s that is the resolution limit of SDSS spectra, there are 74 sample galaxies (18 ULIRGs and 56 LIRGs) with velocity dispersions and r_{50} available from the MPA/JHU catalog. We compare the stellar masses with the dynamical masses for these 74 sample adv-merger (U)LIRGs in the right panel of Figure 7. As can be seen, the stellar masses are systematically smaller than the dynamical masses. In the inset, we compare the distributions of stellar masses and the dynamical masses for the 74 sample (U)LIRGs. The median logarithmic values of the two distributions are 10.84 and 11.06, respectively, indicating that the stellar masses are ~ 0.2 dex smaller than the dynamical masses for sample (U)LIRGs based on the SDSS database.

Given that the above two comparisons based on different datasets yield slightly different results, we compare the data for the 8 overlapping sample (U)LIRGs with dynamical properties measured by Dasyra et al. (2006a, 2006b) and SDSS. We find that the effective radii from Dasyra et al. (2006a, 2006b) are smaller than those of SDSS. In fact, Veilleux et al. (2002) have already found that the effective radii measured in the *K*-band are smaller than those in the *R*-band for *IRAS* 1 Jy ULIRGs samples, due to the extremely dusty environment for the ULIRGs. In contrast, the velocity dispersion measurements have no significant systematic differences from different wavebands (Dasyra et al. 2006b). Therefore, the dynamical masses for 74 sample (U)LIRGs measured by SDSS may be at some level overestimated.

From the comparisons of stellar masses with the dynamical masses from different datasets, we conclude that the stellar masses measured via SED modeling are not over-estimated for our sample (U)LIRGs. Therefore, the adv-merger (U)LIRGs are located in the bottom right corner of the color-mass diagrams.

5.2. Star Formation Rate Estimates

When we investigate the locus of our sample adv-merging (U)LIRGs in the SFR- M_* diagram, the SFRs were estimated using their infrared luminosities. However, Hayward et al. (2014) argued based on their hydrodynamical simulations that for strong starburst galaxies at the post-starburst phase, the instantaneous SFR calculated from the infrared luminosity can be severely over-estimated. This is because the contribution from OB stars to dust heating decreases (the lifetime of OB stars is only 10^6 to 10^7 years) and that from older stellar populations becomes non-negligible when the SFR starts to decrease (e.g., Kennicutt et al. 2009). Therefore the infrared luminosity is not a good indicator of the instantaneous SFR for galaxies at the post-starburst phase, although it is the best SFR tracer for extremely dusty starbursts. On the other hand, the most commonly used $H\alpha$ luminosity can serve as a good SFR indicator for normal star-forming galaxies, for which dust attenuation can be corrected properly. However, for dusty starburst galaxies, massive starbursts tend to take place in obscured circumnuclear regions (K98) where the optical depths are generally an order of magnitude higher than the upper limit of the reddening correction for $H\alpha$ (~ 2.5 mag) (Lonsdale et al. 2006; Moustakas et al. 2006). It is impossible to correct internal dust extinctions accurately for such high optical depths with the Balmer decrements. In such cases, the $H\alpha$ luminosity will under-estimate the real SFRs for dusty starburst galaxies. Given that our galaxy sample consists of both galaxies with transiting post-starburst features (see Section 5.3) and dusty starbursts, it is very likely that the real SFRs of our sample galaxies are in between the SFR(IR) and SFR($H\alpha$). Thus, it is worth investigating the positions of our galaxies on the SFR($H\alpha$)- M_* diagram to see how much will be changed compared to the SFR(IR)- M_* diagram shown in Figure 3.

We plot the SFR($H\alpha$) versus stellar mass in Figure 8, which is the same as Figure 3 except that the $H\alpha$ luminosity is used as the SFR indicator. It is clear from Figure 8 that the positions of our sample (U)LIRGs in the SFR($H\alpha$)- M_* are quite different from those in Figure 3. In particular, ULIRGs are located just above the MS relation and mixed with LIRGs as shown in Figure 8, rather than being apparent outliers as in Figure 3. Even so, most of our dusty adv-merging (U)LIRGs are still located above the MS line in both Figures 3 and 8, for which SFRs are estimated from L_{IR} and $L(H\alpha)$, respectively. Therefore the use

of different SFR indicators does not influence our main conclusions reached in Section 4.1.

5.3. How do Adv-merger (U)LIRGs Evolve on the Color-Mass Diagrams?

The morphologies and locus of our sample adv-merger (U)LIRGs on the SFR(IR)- M_* relation as shown in Figure 3 suggest that most of them are experiencing massive starbursts as triggered by gas-rich major mergers. These galaxies are blue and massive with stellar mass $M_* > 3 \times 10^{10} M_\odot$; they are located to the right of the blue cloud galaxies on the optical and NUV color-mass diagrams, implying that they belong to a distinct population being neither in the blue cloud, red sequence nor the green valley. In spite of the limited data, it is still interesting to investigate how these adv-merger (U)LIRGs may evolve on the color-mass diagrams. To explore this issue, two questions naturally arise: What is the timescale for adv-merger (U)LIRGs exhausting their molecular gas, and then evolving to post-starbursts and finally being quenched? Are there transiting objects from starbursts to post-starbursts among our sample galaxies?

The starburst duration of adv-merger (U)LIRGs can be simply quantified by the gas consumption timescale, i.e., the available gas mass divided by the current SFR. As already pointed out by Daddi et al. (2010) and Genzel et al. (2010) based on CO observations for both low and high redshift galaxies, the molecular gas consumption is bimodal. Disk galaxies consume their gas reservoir slowly, while in starburst galaxies the gas is rapidly exhausted. The fast mode occurs because during a gas-rich major merger gas falls toward the central region and starbursts take place at central kpc rapidly due to high dense gas fractions (Downes & Solomon 1998; Barnes & Hernquist 1996). Given that only 8 of our sample adv-merger (U)LIRGs have existing CO data, we examine the molecular gas depletion timescales mainly based on the adv-merger (U)LIRGs sample by Liu et al. (2015). They collected 66 (U)LIRGs with CO data from the literature and derived their molecular gas masses, out of which 35 (U)LIRGs are adv-merging galaxies. The molecular gas masses of these 35 adv-merging (U)LIRGs plus 6 of our sample (U)LIRGs⁷ are in the range of about $8 \times 10^8 M_\odot$ to $2 \times 10^{10} M_\odot$ where we use the conversion factor (0.8) from the CO luminosity to the molecular gas mass for local (U)LIRGs (Solomon & Vanden Bout 2005). We find the timescale of gas consumption in these adv-merger (U)LIRGs ranges from 3×10^7 to 3×10^8 years, consistent with the rapid star formation mode for starburst galaxies seen by Daddi et al. (2010) and Genzel et al. (2010).

⁷Out of the 8 of our adv-merger (U)LIRGs with existing CO observations, 2 are already included in Liu et al. (2015).

Furthermore, to investigate the link between starbursts and post-starbursts, and to distinguish them from slow quenching normal galaxies, Yesuf et al. (2014) invented two plausible criteria for identifying transiting post-starbursts from a $EW(H\alpha)$ and $EW(H\delta_A)$ restricted⁸ sample: The first is to select the “fading post-starbursts” based on a 3D parameter space constructed by dust-corrected $NUV-g$ color, $EW(H\delta_A)$ as well as the 4000Å break, $D_n(4000)$; the second is to identify the “obscured post-starbursts” using the *GALEX* and *Wide-field Infrared Survey Explore* (*WISE*; Wright et al. 2010) photometry, which is likely the bridge between starbursts and “fading post-starbursts”. Specifically, “fading post-starbursts” are galaxies with more than 2σ deviations from normal galaxy locus in the 3D parameter space constructed by $EW(H\delta_A)$, $D_n(4000)$ and $NUV-g$ color, while the “obscured post-starbursts” are defined as galaxies with $f_{12\mu m}/f_{0.2\mu m} > 200$ and $f_{4.6\mu m}/f_{3.4\mu m} > 0.85$, where $f_{12\mu m}/f_{0.2\mu m}$ is the flux density ratio between *WISE* 12 μm and *GALEX* NUV 0.2 μm , and $f_{4.6\mu m}/f_{3.4\mu m}$ is the flux ratio between *WISE* 4.6 μm and 3.4 μm .

According to the criteria⁹ proposed by Yesuf et al. (2014), there is no “fading post-starbursts” found in our sample. However, based on the *GALEX* and *WISE* photometric data, we identified 12 sample galaxies satisfying the criteria of the “obscured post-starbursts” (see Table 1). From a rough comparison of their SEDs with the stellar population synthesis models, Yesuf et al. (2014) found that the “obscured post-starbursts” have age of about 400-500 Myr since the last starburst epoch, and are younger than the “fading post-starbursts”. Therefore, although most of our sample galaxies are still experiencing massive starbursts, 12 ($\sim 14\%$) of them are in the initial stage of transiting post-starbursts, which is consistent with the theoretical prediction that post-starburst galaxies are the end products of gas-rich major mergers after their gas has been exhausted (Hopkins et al. 2006, 2008).

The short molecular gas depletion timescale along with an appreciable fraction of obscured transiting post-starbursts of our sample favor the scenario that the adv-merger (U)LIRGs follow the fast evolutionary track proposed by several groups (e.g. Muzzin et al. 2013a; Barro et al. 2013, 2014a, 2014b; Marchesini et al. 2014; Schawinski et al. 2014; Belli et al. 2015 and Wellons et al. 2015): the massive gas-rich disk galaxies experience violent merging processes and evolve from the blue cloud galaxies to massive blue and dusty galaxies (from left to right on the color-mass diagram). After the molecular gas has been rapidly exhausted and their star formation ceases, these adv-mergers become massive red-sequence galaxies through the transiting post-starburst phase within ~ 1 Gyr.

⁸ $3\text{\AA} < EW(H\alpha) < 175\text{\AA}$ and $EW(H\delta_A) > 4\text{\AA}$

⁹Instead of using the $NUV-g$ color, we use our dust-corrected $NUV-r$ color measurements for the selection of “fading post-starbursts” for convenience.

6. SUMMARY

With the aim of exploring the evolutionary pathway from the blue cloud of star-forming galaxies to the red sequence of quiescent galaxies, we use a local adv-merger (U)LIRGs sample and apply careful dust extinction corrections to investigate their positions in the SFR- M_* , $u-r$ and $NUV-r$ color-mass diagrams. Our sample consists of 89 luminous infrared and ultraluminous infrared galaxies at the late merger stage, which has been obtained from cross-correlating the *IRAS* PSCz and 1 Jy ULIRGs samples with the SDSS DR7 database. Our main results are summarized as follows.

1. We find that almost all adv-merger (U)LIRGs are located above the local star-forming galaxy main sequence (MS) in the SFR- M_* diagram. Specifically, the ULIRGs are far above the MS line as outliers and $62\% \pm 6\%$ LIRGs are above the 1σ line of the MS, indicating that a majority (two-thirds) of these gas-rich major merger galaxies at the late merging stage are at the starburst stage with high star formation rates.
2. We also find that almost all our sample adv-merger (U)LIRGs are as blue as the blue cloud galaxies after carefully removing the Galactic and internal dust extinctions. They are also massive and thus localized to the right of the blue cloud galaxies on the $u-r$ and $NUV-r$ color-mass diagrams with $95\% \pm 2\%$ and $81\% \pm 4\%$ sample galaxies outside the 90% density contour of blue cloud galaxies, respectively. Therefore, the adv-merger (U)LIRGs are a distinct population in the color-mass diagram that differ from the blue cloud, green valley, and red sequence galaxies. However, these galaxies are rare in the local universe and their number density is only $\sim 0.1\%$ of that of the local blue cloud galaxies. In contrast, the fraction of similar objects at high redshift is much larger (7%) (see Straatman et al. 2015).

The molecular gas depletion timescale for adv-merger (U)LIRGs is 3×10^7 to 3×10^8 years, which is much shorter than that for disk galaxies in the blue cloud. We also identified 12 ($\sim 14\%$) obscured transiting post-starbursts based on the *GALEX* and *WISE* photometry following Yesuf et al. (2014), implying that more than ten percent of adv-merger (U)LIRGs are at the initial stage of transiting post-starbursts. Therefore, our results favor the fast evolutionary track proposed by several groups (e.g. Marchesini et al. 2009, 2014; Brammer et al. 2011; Muzzin et al. 2013a; Barro et al. 2013, 2014a, 2014b; Schawinski et al. 2014; Belli et al. 2015; Mancini et al. 2015) that massive disk galaxies experience violent merger processes and evolve from the blue cloud first to the massive blue and dusty galaxies, and then rapidly to the red sequence through the green valley and eventually form massive quiescent galaxies. Given that the merger rate and gas fraction are much higher for high

redshift galaxies, this evolutionary track must be an important channel for the formation of massive red sequence galaxies over the cosmic time.

We would like to thank the anonymous referee for several constructive reports that improved the manuscript. We also thank Drs. Yu Gao, Haojing Yan, Jiasheng Huang and Sandy Faber for advice and helpful discussions. This project is supported by the NSF of China 11373027, 10973011, 11333003 and 11390372. It has also been supported by the Strategic Priority Research Program “The Emergence of Cosmological Structures” of the Chinese Academy of Sciences Grant No. XDB09000000 (SM). Funding for the creation and distribution of the SDSS Archive has been provided by the Alfred P. Sloan Foundation, the Participating Institutions, the National Aeronautics and Space Administration, the National Science Foundation, the U.S. Department of Energy, the Japanese Monbukagakusho, and the Max Planck Society. The SDSS Web site is <http://www.sdss.org/>. The SDSS is managed by the Astrophysical Research Consortium (ARC) for the Participating Institutions. The Participating Institutions are The University of Chicago, Fermilab, the Institute for Advanced Study, the Japan Participation Group, The Johns Hopkins University, the Korean Scientist Group, Los Alamos National Laboratory, the Max-Planck-Institute for Astronomy (MPIA), the Max-Planck-Institute for Astrophysics (MPA), New Mexico State University, University of Pittsburgh, Princeton University, the United States Naval Observatory, and the University of Washington. Some of the data presented in this paper were obtained from the Mikulski Archive for Space Telescopes (MAST). STScI is operated by the Association of Universities for Research in Astronomy, Inc., under NASA contract NAS5-26555. Support for MAST for non-HST data is provided by the NASA Office of Space Science via grant NNX09AF08G and by other grants and contracts. This publication makes use of data products from the Wide-field Infrared Survey Explorer, which is a joint project of the University of California, Los Angeles, and the Jet Propulsion Laboratory/California Institute of Technology, funded by the National Aeronautics and Space Administration.

REFERENCES

- Abazajian, K. N., Adelman-McCarthy, J. K., Agüeros, M. A., et al. 2009, *ApJS*, 182, 543
- Ahn, C. P., Alexandroff, R., Allende Prieto, C., et al. 2014, *ApJS*, 211, 17
- Baldry, I. K., Balogh, M. L., Bower, R. G., et al. 2006, *MNRAS*, 373, 469
- Baldry, I. K., Glazebrook, K., Brinkmann, J., et al. 2004, *ApJ*, 600, 681
- Baldwin, J. A., Phillips, M. M., & Terlevich, R. 1981, *PASP*, 93, 5

- Barnes, J. E., & Hernquist, L. 1996, *ApJ*, 471, 115
- Barro, G., Faber, S. M., Pérez-González, P. G., et al. 2014a, *ApJ*, 791, 52
- Barro, G., Faber, S. M., Pérez-González, P. G., et al. 2013, *ApJ*, 765, 104
- Barro, G., Trump, J. R., Koo, D. C., et al. 2014b, *ApJ*, 795, 145
- Bell, E. F., McIntosh, D. H., Katz, N., & Weinberg, M. D. 2003, *ApJS*, 149, 289
- Bell, E. F., Wolf, C., Meisenheimer, K., et al. 2004, *ApJ*, 608, 752
- Belli, S., Newman, A. B., & Ellis, R. S. 2015, *ApJ*, 799, 206
- Bernardi, M., Shankar, F., Hyde, J. B., et al. 2010, *MNRAS*, 404, 2087
- Blanton, M. R., Eisenstein, D., Hogg, D. W., Schlegel, D. J., & Brinkmann, J. 2005, *ApJ*, 629, 143
- Blanton, M. R., & Roweis, S. 2007, *AJ*, 133, 734
- Bouwens, R. J., Illingworth, G. D., Oesch, P. A., et al. 2012, *ApJ*, 754, 83
- Brammer, G. B., Whitaker, K. E., van Dokkum, P. G., et al. 2011, *ApJ*, 739, 24
- Brinchmann, J., Charlot, S., White, S. D. M., et al. 2004, *MNRAS*, 351, 1151
- Calzetti, D., Armus, L., Bohlin, R. C., et al. 2000, *ApJ*, 533, 682
- Cardelli, J. A., Clayton, G. C., & Mathis, J. S. 1989, *ApJ*, 345, 245
- Casey, C. M., Scoville, N. Z., Sanders, D. B., et al. 2014, *ApJ*, 796, 95
- Chen, Y., Lowenthal, J. D., & Yun, M. S. 2010, *ApJ*, 712, 1385
- Chilingarian, I. V., Melchior, A.-L., & Zolotukhin, I. Y. 2010, *MNRAS*, 405, 1409
- Chilingarian, I. V., & Zolotukhin, I. Y. 2012, *MNRAS*, 419, 1727
- Colless, M., Dalton, G., Maddox, S., et al. 2001, *MNRAS*, 328, 1039
- Cortese, L. 2012, *A&A*, 543, A132
- da Cunha, E., Charmandaris, V., Díaz-Santos, T., et al. 2010, *A&A*, 523, A78
- Daddi, E., Elbaz, D., Walter, F., et al. 2010, *ApJ*, 714, L118

- Darling, J., & Giovanelli, R. 2006, *AJ*, 132, 2596
- Dasyra, K. M., Tacconi, L. J., Davies, R. I., et al. 2006a, *ApJ*, 638, 745
- Dasyra, K. M., Tacconi, L. J., Davies, R. I., et al. 2006b, *ApJ*, 651, 835
- Downes, D., & Solomon, P. M. 1998, *ApJ*, 507, 615
- Elbaz, D., Daddi, E., Le Borgne, D., et al. 2007, *A&A*, 468, 33
- Faber, S. M., Willmer, C. N. A., Wolf, C., et al. 2007, *ApJ*, 665, 265
- Fukugita, M., Nakamura, O., Turner, E. L., Helmboldt, J., & Nichol, R. C. 2004, *ApJ*, 601, L127
- Gao, Y., & Solomon, P. M. 2004, *ApJ*, 606, 271
- Genzel, R., Tacconi, L. J., Gracia-Carpio, J., et al. 2010, *MNRAS*, 407, 2091
- Goto, T., Arnouts, S., Malkan, M., et al. 2011, *MNRAS*, 414, 1903
- Grogin, N. A., Kocevski, D. D., Faber, S. M., et al. 2011, *ApJS*, 197, 35
- Hayward, C. C., Lanz, L., Ashby, M. L. N., et al. 2014, *MNRAS*, 445, 1598
- Hopkins, A. M., Miller, C. J., Nichol, R. C., et al. 2003, *ApJ*, 599, 971
- Hopkins, P. F., Hernquist, L., Cox, T. J., et al. 2006, *ApJS*, 163, 1
- Hopkins, P. F., Hernquist, L., Cox, T. J., & Kereš, D. 2008, *ApJS*, 175, 356-389
- Hung, C.-L., Sanders, D. B., Casey, C. M., et al. 2013, *ApJ*, 778, 129
- Hung, C.-L., Sanders, D. B., Casey, C. M., et al. 2014, *ApJ*, 791, 63
- Ilbert, O., Salvato, M., Le Floc’h, E., et al. 2010, *ApJ*, 709, 644
- Kartaltepe, J. S., Dickinson, M., Alexander, D. M., et al. 2012, *ApJ*, 757, 23
- Kartaltepe, J. S., Sanders, D. B., Le Floc’h, E., et al. 2010, *ApJ*, 721, 98
- Kauffmann, G., Heckman, T. M., Tremonti, C., et al. 2003a, *MNRAS*, 346, 1055
- Kauffmann, G., Heckman, T. M., White, S. D. M., et al. 2003b, *MNRAS*, 341, 33
- Kauffmann, G., White, S. D. M., Heckman, T. M., et al. 2004, *MNRAS*, 353, 713

- Kaviraj, S. 2009, MNRAS, 394, 1167
- Kennicutt, R. C., Jr. 1998, ARA&A, 36, 189
- Kennicutt, R. C., Jr., Hao, C.-N., Calzetti, D., et al. 2009, ApJ, 703, 1672
- Kewley, L. J., Dopita, M. A., Sutherland, R. S., Heisler, C. A., & Trevena, J. 2001, ApJ, 556, 121
- Kilerci Eser, E., Goto, T., & Doi, Y. 2014, ApJ, 797, 54
- Kim, D.-C., & Sanders, D. B. 1998, ApJS, 119, 41
- Kim, D.-C., Veilleux, S., & Sanders, D. B. 2002, ApJS, 143, 277
- Knapen, J. H., & James, P. A. 2009, ApJ, 698, 1437
- Koekemoer, A. M., Faber, S. M., Ferguson, H. C., et al. 2011, ApJS, 197, 36
- Kriek, M., van Dokkum, P. G., Franx, M., Illingworth, G. D., & Magee, D. K. 2009, ApJ, 705, L71
- Kroupa, P. 2001, MNRAS, 322, 231
- Lee, J. C., Hwang, H. S., & Ko, J. 2013, ApJ, 774, 62
- Leitner, S. N. 2012, ApJ, 745, 149
- Lintott, C., Schawinski, K., Bamford, S., et al. 2011, MNRAS, 410, 166
- Lintott, C. J., Schawinski, K., Slosar, A., et al. 2008, MNRAS, 389, 1179
- Liu, L., Gao, Y., & Greve, T. R. 2015, ApJ, 805, 31
- Lonsdale, C. J., Farrah, D., & Smith, H. E. 2006, Astrophysics Update 2 (Praxis Publishing Ltd, Chichester, UK), 285
- Lupton, R., Blanton, M. R., Fekete, G., et al. 2004, PASP, 116, 133
- Magdis, G. E., Rigopoulou, D., Huang, J.-S., & Fazio, G. G. 2010, MNRAS, 401, 1521
- Mancini, C., Renzini, A., Daddi, E., et al. 2015, MNRAS, 450, 763
- Marchesini, D., Muzzin, A., Stefanon, M., et al. 2014, ApJ, 794, 65
- Marchesini, D., van Dokkum, P. G., Förster Schreiber, N. M., et al. 2009, ApJ, 701, 1765

- Martin, D. C., Fanson, J., Schiminovich, D., et al. 2005, *ApJ*, 619, L1
- Martin, D. C., Wyder, T. K., Schiminovich, D., et al. 2007, *ApJS*, 173, 342
- McIntosh, D. H., Wagner, C., Cooper, A., et al. 2014, *MNRAS*, 442, 533
- Moustakas, J., Kennicutt, R. C., Jr., & Tremonti, C. A. 2006, *ApJ*, 642, 775
- Murakami, H., Baba, H., Barthel, P., et al. 2007, *PASJ*, 59, S369
- Muzzin, A., Marchesini, D., Stefanon, M., et al. 2013a, *ApJ*, 777, 18
- Muzzin, A., Marchesini, D., Stefanon, M., et al. 2013b, *ApJS*, 206, 8
- Nakamura, O., Fukugita, M., Yasuda, N., et al. 2003, *AJ*, 125, 1682
- Noeske, K. G., Weiner, B. J., Faber, S. M., et al. 2007, *ApJ*, 660, L43
- Oh, K., Sarzi, M., Schawinski, K., & Yi, S. K. 2011, *ApJS*, 195, 13
- Osterbrock, D. E., & Ferland, G. J. 2006, *Astrophysics of gaseous nebulae and active galactic nuclei*, 2nd. ed. by D.E. Osterbrock and G.J. Ferland. Sausalito, CA: University Science Books, 2006,
- Rodighiero, G., Daddi, E., Baronchelli, I., et al. 2011, *ApJ*, 739, L40
- Rodríguez Zaurín, J., Holt, J., Tadhunter, C. N., & González Delgado, R. M. 2007, *MNRAS*, 375, 1133
- Rodríguez Zaurín, J., Tadhunter, C. N., & González Delgado, R. M. 2008, *MNRAS*, 384, 875
- Salim, S., Rich, R. M., Charlot, S., et al. 2007, *ApJS*, 173, 267
- Salmon, B., Papovich, C., Finkelstein, S. L., et al. 2015, *ApJ*, 799, 183
- Salpeter, E. E. 1955, *ApJ*, 121, 161
- Sanders, D. B., & Mirabel, I. F. 1996, *ARA&A*, 34, 749
- Sargent, M. T., Béthermin, M., Daddi, E., & Elbaz, D. 2012, *ApJ*, 747, L31
- Saunders, W., Sutherland, W. J., Maddox, S. J., et al. 2000, *MNRAS*, 317, 55
- Schawinski, K., Urry, C. M., Simmons, B. D., et al. 2014, *MNRAS*, 440, 889

- Schiminovich, D., Wyder, T. K., Martin, D. C., et al. 2007, *ApJS*, 173, 315
- Schlegel, D. J., Finkbeiner, D. P., & Davis, M. 1998, *ApJ*, 500, 525
- Solomon, P. M., & Vanden Bout, P. A. 2005, *ARA&A*, 43, 677
- Soto, K. T., & Martin, C. L. 2012, *ApJS*, 203, 3
- Straatman, C. M. S., Labbé, I., Spitler, L. R., et al. 2015, *ApJ*, 808, L29
- van Dokkum, P. G., Franx, M., Kriek, M., et al. 2008, *ApJ*, 677, L5
- Veilleux, S., Kim, D.-C., & Sanders, D. B. 2002, *ApJS*, 143, 315
- Veilleux, S., Kim, D.-C., & Sanders, D. B. 1999, *ApJ*, 522, 113
- Wang, J. L., Xia, X. Y., Mao, S., et al. 2006, *ApJ*, 649, 722
- Wellons, S., Torrey, P., Ma, C.-P., et al. 2015, *MNRAS*, 449, 361
- Whitaker, K. E., van Dokkum, P. G., Brammer, G., & Franx, M. 2012, *ApJ*, 754, L29
- Wright, E. L., Eisenhardt, P. R. M., Mainzer, A. K., et al. 2010, *AJ*, 140, 1868-1881
- Wyder, T. K., Martin, D. C., Schiminovich, D., et al. 2007, *ApJS*, 173, 293
- Yan, H., Stefanon, M., Ma, Z., et al. 2014, *ApJS*, 213, 2
- Yesuf, H. M., Faber, S. M., Trump, J. R., et al. 2014, *ApJ*, 792, 84
- York, D. G., Adelman, J., Anderson, J. E., Jr., et al. 2000, *AJ*, 120, 1579
- Zamojski, M., Yan, L., Dasyra, K., et al. 2011, *ApJ*, 730, 125

Table 1. Physical Parameters for the Classification of “Obscured Post-Starbursts”

Source (1)	EW(H α) ^a (2)	EW(H δ_A) (3)	$f_{12\mu m}/f_{0.2\mu m}$ (4)	$f_{4.6\mu m}/f_{3.4\mu m}$ (5)
Q14168+0153	56.96 \pm 4.13	5.90 \pm 0.31	290.34 \pm 9.89	1.01 \pm 0.03
Q15257+0302	129.53 \pm 8.14	4.34 \pm 0.61	322.77 \pm 18.76	0.97 \pm 0.03
Q22364+1256	132.46 \pm 25.56	7.12 \pm 0.72	762.41 \pm 30.78	0.86 \pm 0.03
Q12383+2749	141.91 \pm 8.15	6.69 \pm 0.30	403.53 \pm 15.82	1.54 \pm 0.04
Q13293+0216	157.88 \pm 15.01	6.21 \pm 0.32	557.06 \pm 35.51	1.76 \pm 0.05
Q08550+3908	173.04 \pm 16.91	4.22 \pm 0.97	411.68 \pm 66.84	1.12 \pm 0.03
Q09343+6450	162.17 \pm 17.82	4.88 \pm 0.55	1674.52 \pm 143.05	0.86 \pm 0.02
Q15233+0533	88.54 \pm 8.51	6.95 \pm 0.38	377.91 \pm 24.92	0.88 \pm 0.02
F08559+1053	145.12 \pm 12.82	4.91 \pm 0.60	1142.33 \pm 136.60	1.47 \pm 0.04
F08591+5248	110.89 \pm 11.40	6.65 \pm 0.58	666.50 \pm 42.29	0.99 \pm 0.03
F09039+0503	138.04 \pm 13.94	4.13 \pm 0.78	262.73 \pm 15.15	1.02 \pm 0.04
F11387+4116	129.25 \pm 27.68	5.53 \pm 0.87	821.24 \pm 81.18	0.95 \pm 0.03

^aSince the MPA/JHU catalog cautions the correctness of the H α continuum uncertainties, we re-measured them to derive the uncertainties of the EW(H α).



Fig. 1.— True color images of 8 example adv-mergers with tidal tails or other merging signatures, constructed from SDSS (g , r , i) images following Lupton et al. (2004). The top row shows 4 LIRGs and the bottom row shows 4 ULIRGs. The physical size of each image is 80×80 kpc².

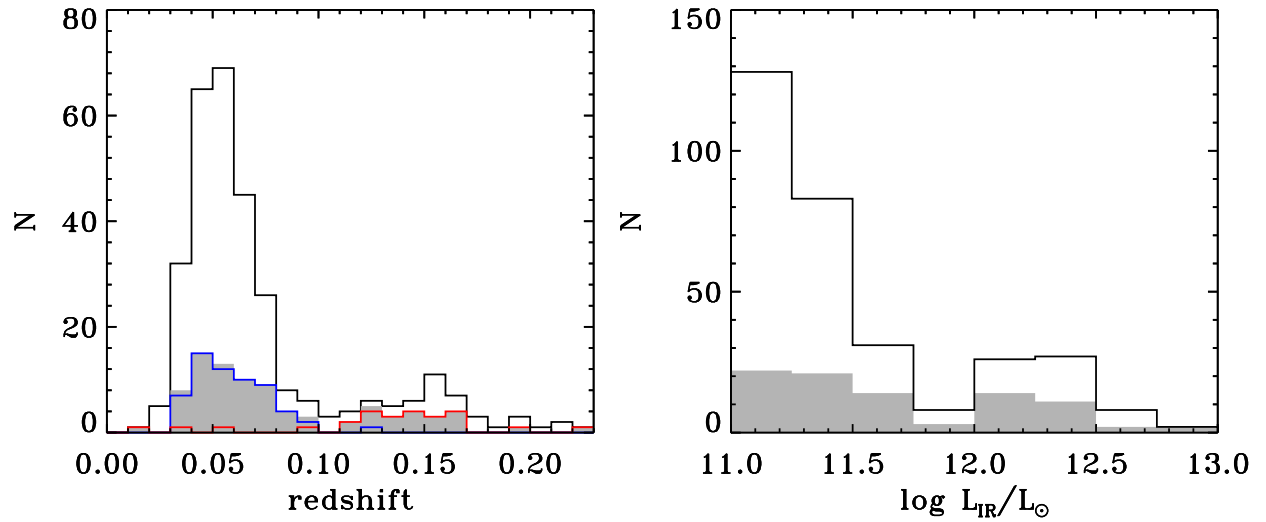


Fig. 2.— Redshift and infrared luminosity distributions for (U)LIRGs. The black histograms denote the 314 (U)LIRGs from cross-correlation analysis, while the gray shaded histograms represent the 89 adv-merger (U)LIRGs. The blue and red histograms in the left panel represent the redshift distributions of LIRGs and ULIRGs respectively.

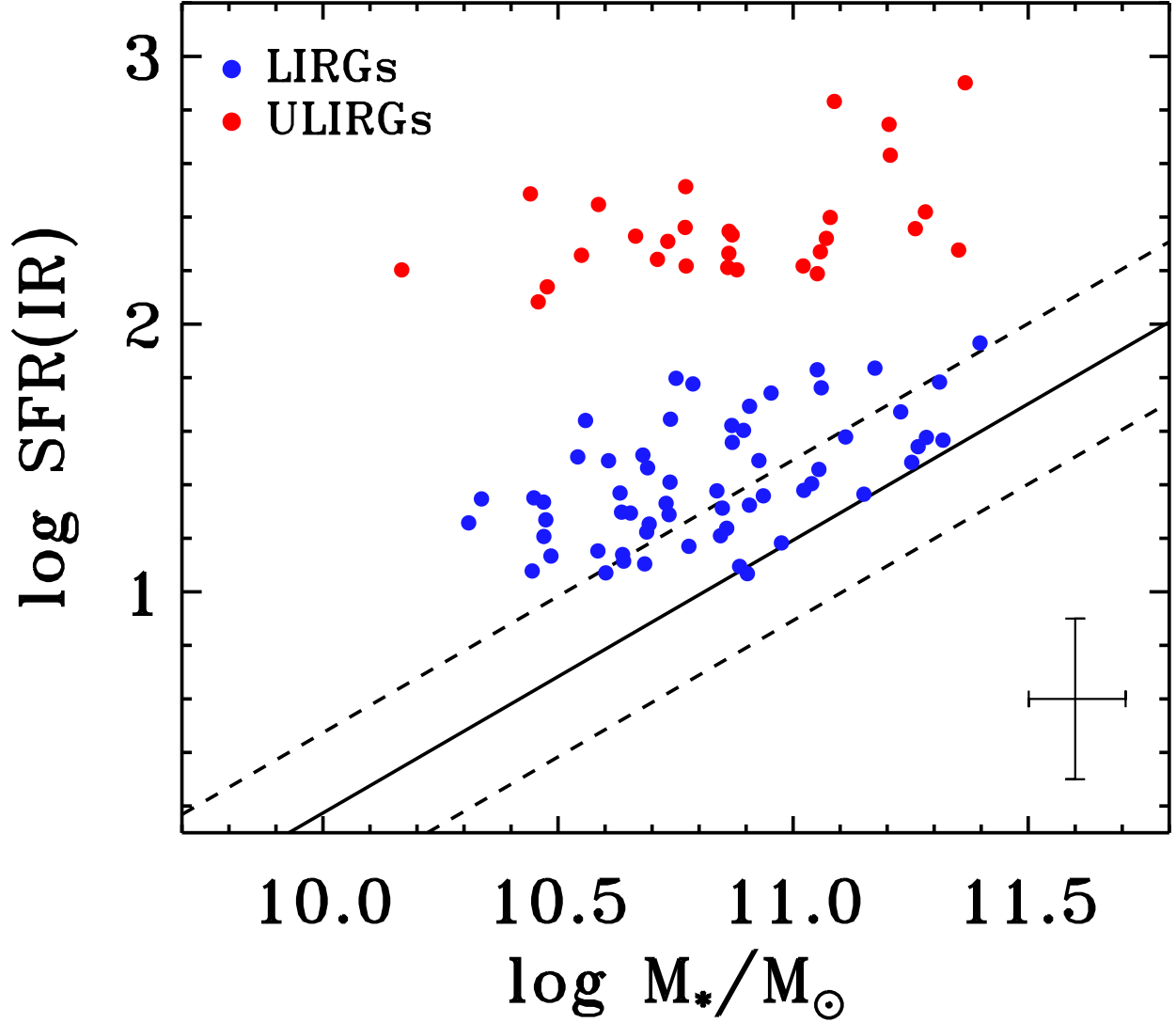


Fig. 3.— SFR(IR) vs. stellar mass relation for our sample adv-mergers. Blue and red filled circles represent LIRGs and ULIRGs, respectively. The error bars show the median uncertainties. The black solid line is the local main sequence (MS) relation based on 152137 star-forming galaxies of SDSS DR7 and SFR($\text{H}\alpha$) are used. The dashed lines show the 1σ dispersions (0.3 dex) from the MS fitting.

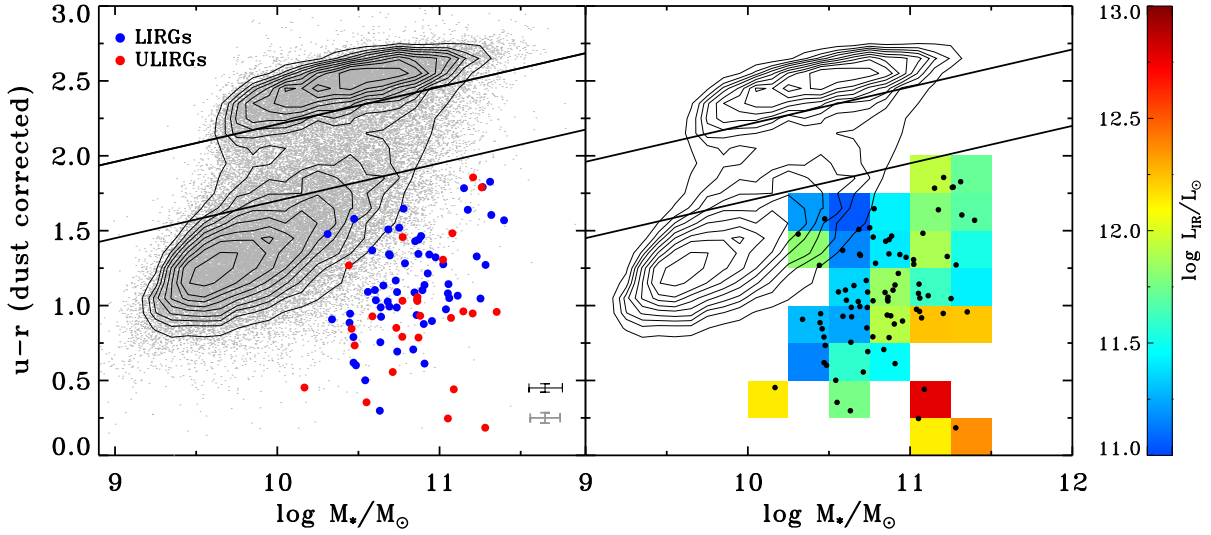


Fig. 4.— Left panel: dust-corrected $u-r$ color-mass diagram for sample adv-mergers. Blue and red filled circles represent LIRGs and ULIRGs, respectively. The contours show 9 equally spaced levels between 10% and 90% number densities of galaxies drawn from SDSS DR7 (gray dots). The black and gray error bars show the median uncertainties for the sample adv-mergers and the control sample galaxies, respectively. The black solid lines are taken from Schawinski et al. (2014) as the separation between the blue cloud, green valley and red sequence and have been shifted downward by 0.07 mag to account for foreground Galactic extinction correction. Right panel: same as the left panel but with the L_{IR} distribution of these adv-mergers overlaid. The color scale of L_{IR} is shown to the right.

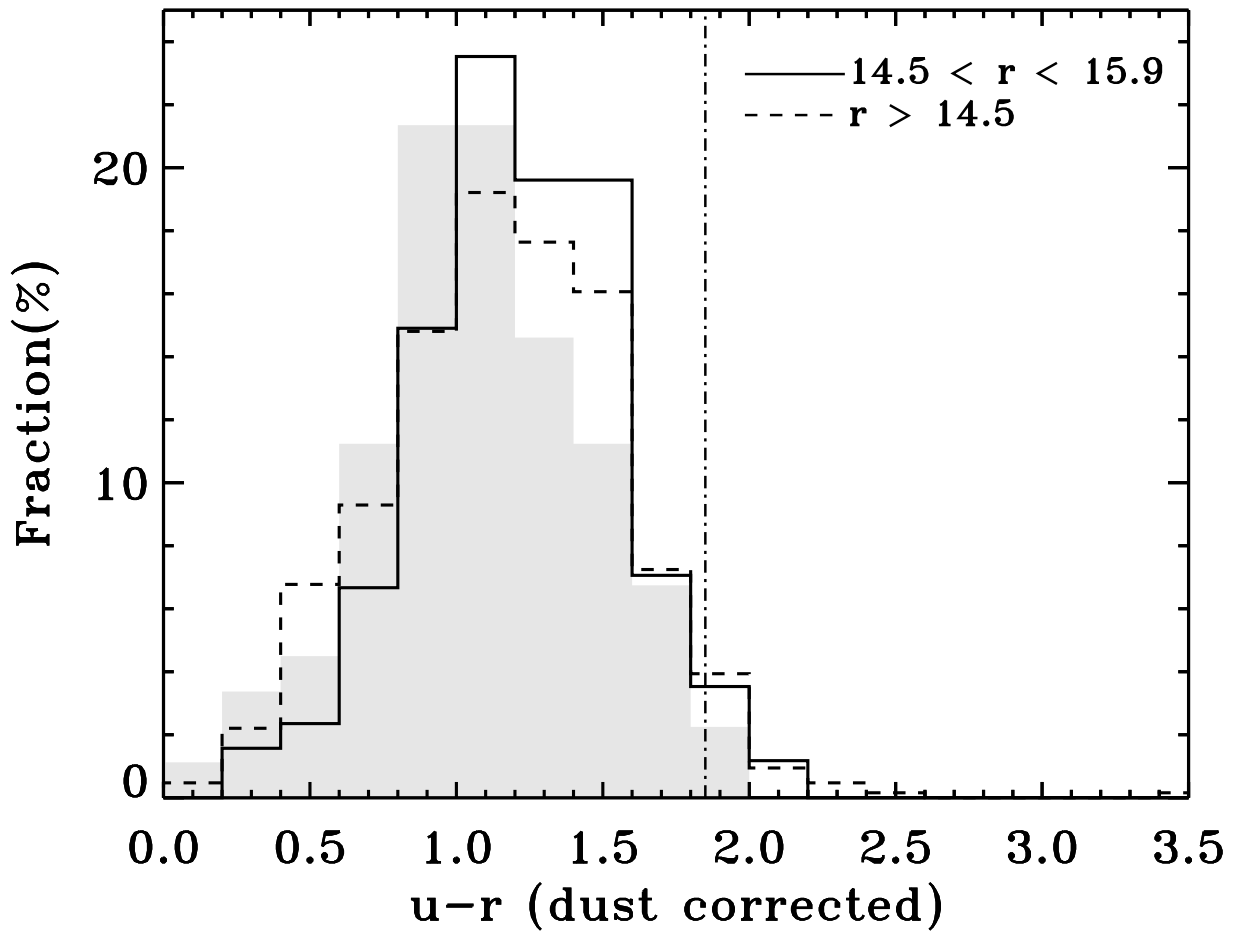


Fig. 5.— Comparisons of the $u-r$ color distributions between the (U)LIRGs selected from the cross-correlation analysis with $14.5 < r < 15.9$ (solid line) and those with $r > 14.5$ (dashed line). The gray shaded histogram represents the 89 sample adv-merger (U)LIRGs. The black vertical dot-dashed line denotes the color of the lower boundary of the green valley at the median stellar mass of our sample galaxies.

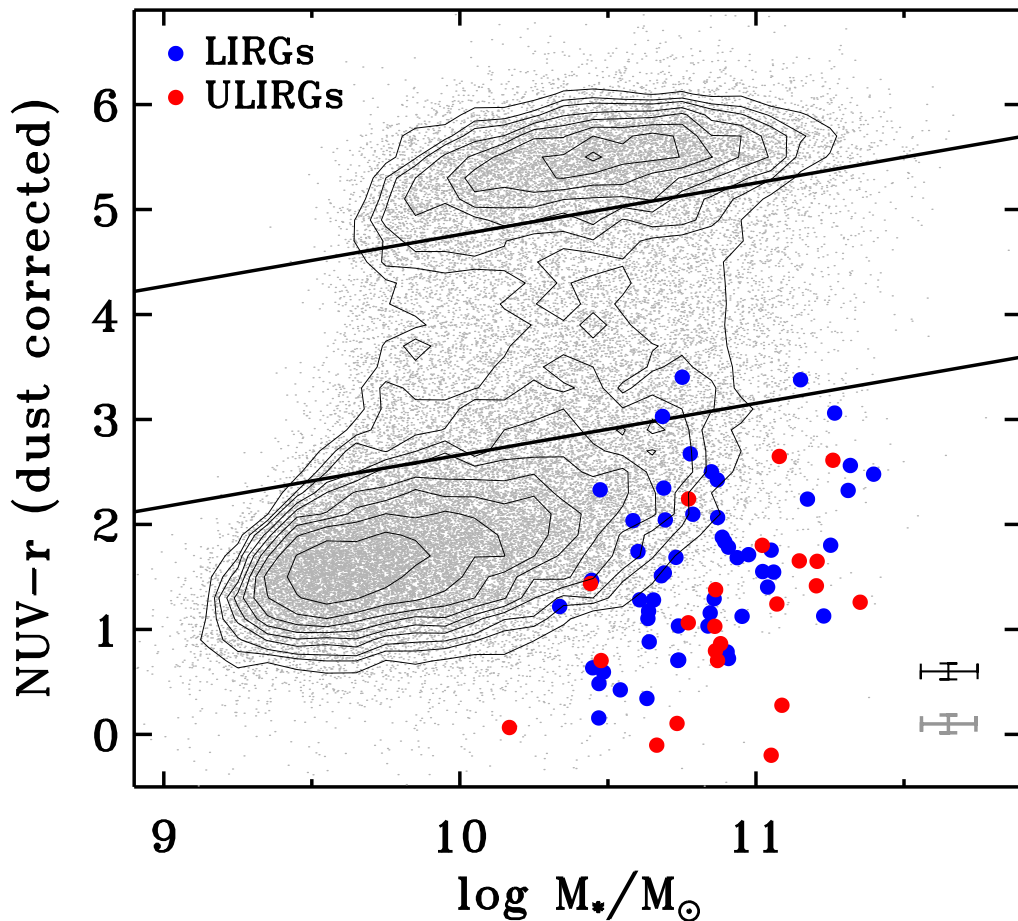


Fig. 6.— Dust-corrected $NUV-r$ color-mass diagram for sample adv-mergers with NUV photometry from *GALEX*. Blue and red filled circles represent LIRGs and ULIRGs, respectively. The contours show 9 equally spaced levels between 10% and 90% number densities of 46407 galaxies drawn from SDSS DR7 with NUV photometry (gray dots). The black and gray error bars show the median uncertainties for the sample adv-mergers and the control sample galaxies, respectively. The black solid lines indicate the boundaries of the green valley according to Equations (7) and (8).

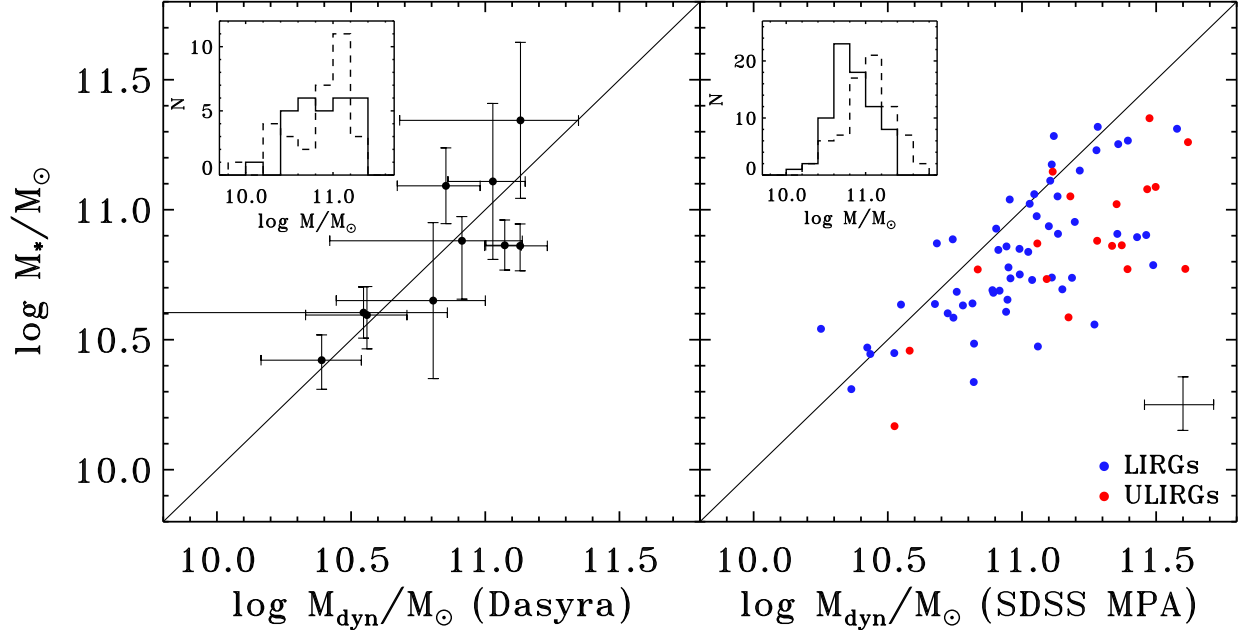


Fig. 7.— Comparisons between the stellar masses (M_*) and the dynamical masses (M_{dyn}). Left panel: M_* vs. M_{dyn} for 10 overlapping ULIRGs between Dasyra et al. (2006a, 2006b) and our sample. The solid line represents the line of equality. The error bars show the uncertainties for each individual points. The inset histograms show the distributions of M_* for our 29 sample ULIRGs (solid line) and the M_{dyn} for 31 ULIRGs with single nucleus from Dasyra et al. (2006b) (dashed line). The median logarithmic values of these two distributions are 10.86 and 10.91 respectively. Right panel: M_* vs. M_{dyn} for 74 sample adv-merger (U)LIRGs with velocity dispersions from the MPA/JHU catalog. The blue and red dots represent LIRGs and ULIRGs, respectively. The solid line represents the line of equality. The error bars show the median uncertainties. The inset histograms show the distributions of M_* (solid line) and M_{dyn} (dashed line) for the 74 sample adv-merger (U)LIRGs. The median values of these two distributions for $\log M_*/M_\odot$ and $\log M_{\text{dyn}}/M_\odot$ are 10.84 and 11.06, respectively.

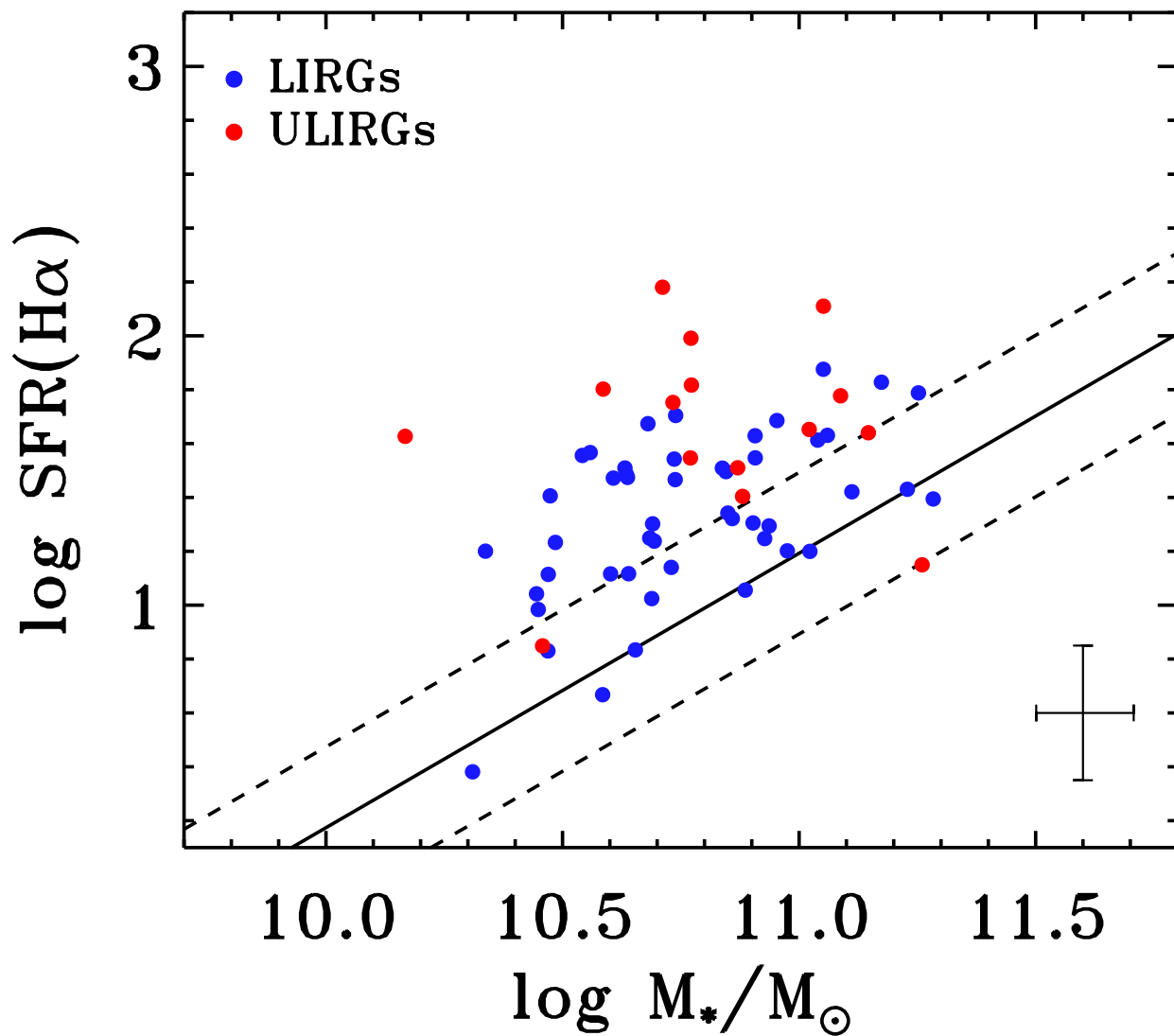


Fig. 8.— SFR($\text{H}\alpha$) vs. stellar mass relation for star-forming and composite sample adv-mergers. The main sequence (MS) line and symbols are the same as in Figure 3. The median error bars are shown in the bottom right.